

Kinetic evaluation and assessment of longitudinal changes in reference region and extracerebral [¹⁸F]MK-6240 PET uptake

Jessie Fanglu Fu^{1,2,*} , Cristina Lois^{2,3,*}, Justin Sanchez³, J Alex Becker^{2,3}, Zoe B Rubinstein³, Emma Thibault³, Andrew N Salvatore¹, Hasan Sari^{1,2}, Michelle E Farrell², Nicolas J Guehl^{2,3}, Marc D Normandin^{2,3}, Georges El Fakhri^{2,3}, Keith A Johnson^{2,3} and Julie C Price^{1,2}

Abstract

[¹⁸F]MK-6240 meningeal/extracerebral off-target binding may impact tau quantification. We examined the kinetics and longitudinal changes of extracerebral and reference regions. [¹⁸F]MK-6240 PET was performed in 24 cognitively-normal and eight cognitively-impaired subjects, with arterial samples in 13 subjects. Follow-up scans at 6.1 ± 0.5 ($n = 25$) and 13.3 ± 0.9 ($n = 16$) months were acquired. Extracerebral and reference region (cerebellar gray matter (CerGM)-based, cerebral white matter (WM), pons) uptake were evaluated using standardized uptake values (SUV_{90-110}), spectral analysis, and distribution volume. Longitudinal changes in SUV_{90-110} were examined. The impact of reference region on target region outcomes, partial volume correction (PVC) and regional erosion were evaluated. Eroded WM and pons showed lower variability, lower extracerebral contamination, and lower longitudinal changes than CerGM-based regions. CerGM-based regions resulted larger cross-sectional effect sizes for group differentiation. Extracerebral signal was high in 50% of subjects and exhibited irreversible kinetics and nonsignificant longitudinal changes over one-year but was highly variable at subject-level. PVC resulted in higher variability in reference region uptake and longitudinal changes. Our results suggest that eroded CerGM may be preferred for cross-sectional, whilst eroded WM or pons may be preferred for longitudinal [¹⁸F]MK-6240 studies. For CerGM, erosion was necessary (preferred over PVC) to address the heterogenous nature of extracerebral signal.

Keywords

[¹⁸F]MK-6240, extracerebral signal, positron emission tomography, reference tissue modeling, tau

Received 19 June 2022; Revised 17 October 2022; Accepted 6 November 2022

Introduction

The accumulation of neurofibrillary tangles consisting of hyperphosphorylated tau protein is one of the neuropathological hallmarks of Alzheimer's disease (AD). Tau accumulation in the brain can be quantified *in-vivo* with positron emission tomography (PET). [¹⁸F]MK-6240, a second-generation tau PET radioligand, has demonstrated high affinity ($K_d \sim 0.3$ nM) for AD tauopathies, lower off-target binding in basal ganglia than first-generation radioligands, and spatial distribution in the brain consistent with the neuropathological

¹Athinoula A. Martinos Center for Biomedical Imaging, Massachusetts General Hospital, Charlestown, MA, USA

²Harvard Medical School, Department of Radiology, Boston, MA, USA

³Gordon Center for Medical Imaging, Massachusetts General Hospital, Boston, MA, USA

*Authors contributed equally to this work.

Corresponding author:

Jessie Fanglu Fu, Bldg 149, 13 Street, Charlestown, MA 02129, USA.
Email: ffu@mgh.harvard.edu

staging of tau accumulation in AD brains.^{1–5} Several studies have demonstrated the applicability of [¹⁸F]MK-6240 in subjects with mild cognitive impairment (MCI) and AD.^{4,6–8} However, off-target binding to melanin-containing cells, especially in the meningeal space (i.e., extracerebral signal), has been observed in both *in-vivo* imaging and post-mortem studies.^{5,6,8,9} The physiological and kinetic properties of the extracerebral signal are not yet well understood, and extracerebral spill-in contamination into the brain may hamper accurate quantification of tau-specific uptake.

The gold standard for quantifying radioligand-protein binding requires kinetic modeling with arterial blood sampling. Since this method entails technical and participant burden, semi-quantitative reference-tissue methods are often preferred, under the assumption that the reference region is: (1) devoid of specific binding, (2) representative of non-displaceable binding in the target regions, and (3) unaffected by disease or treatment.^{6,8,10} The cerebellar gray matter (CerGM) has been shown to have kinetics consistent with non-displaceable uptake across cognitively normal (CN) and AD/MCI subjects and thus, was suggested as a potential reference region for [¹⁸F]MK-6240 quantification.^{4,5} However, uptake in the CerGM may be contaminated by spill-in uptake signal from the extracerebral region and from the occipital and temporal cortices. To address these challenges, several studies utilized alternative reference regions, including the inferior cerebellar gray matter (InfCer) and CerGM with an erosion of the outer regional voxels^{2,4,6–8,11–18} (Supplementary Table.1). Studies with [¹⁸F]Flortaucipir and amyloid- β (A β) radioligands evaluated pons and cerebral white matter (WM) as reference regions, reporting increased sensitivity for detecting longitudinal changes in radiotracer uptake in target regions compared to CerGM-based reference regions.^{19–23} Pons and cerebral WM were also suggested to be less affected by scanner sensitivity non-uniformity along the transaxial axis and different reconstruction methods.^{24,25} Furthermore, due to the more central anatomical location within the brain, the pons is also less vulnerable to signal spill-in from cortical and extracerebral uptake. Previous [¹⁸F]MK-6240 studies examined the pons time-activity data and showed consistent kinetics across CN and AD/MCI subjects^{2,4} but selected the CerGM as the reference region for further reference-tissue analyses due to its larger size.

Despite the increasing application of [¹⁸F]MK-6240 PET, comparative evaluations of potential reference regions have been limited. In this study, we investigate the *in-vivo* kinetics of [¹⁸F]MK-6240 uptake in three types of potential reference regions (CerGM-based, cerebral WM-based, and pons) and in the extracerebral region using spectral analysis and arterial-based kinetic

analyses. We then examine longitudinal changes in the reference region and extracerebral uptake up to one year after the baseline study. Lastly, we evaluate the impact of the reference region on the quantification of tau load in target regions in reference tissue-based analyses, and on detecting biological effects. This work is a first step in the investigation of factors that may impact the robust detection of early tau deposition in target regions, and future work will more comprehensively examine how these propagate to longitudinal changes in target region uptake.

Materials and methods

Study participants

Subjects were recruited at the Massachusetts General Hospital (MGH) and underwent comprehensive medical and neurological evaluations. All subjects provided written informed consent, as approved by the local institutional review board.^{6,19} The study included eight cognitively impaired subjects (six with MCI and two with AD) and 24 age-matched CN. The diagnostic status of each participant was determined clinically by established criteria described by Albert et al.²⁶ The A β status of all subjects was determined using [¹¹C] Pittsburgh Compound B (PiB) PET with a threshold of 1.13 using gaussian mixture model²⁰ (see details in the Supplementary Materials). The tau status was determined using a SUVR₉₀₋₁₁₀ threshold of 1.35 in the temporal meta-ROI (comprised of entorhinal cortex, amygdala, inferior temporal, fusiform and parahippocampus) as described in a recent [¹⁸F]MK-6240 study.¹⁶ Twenty-five subjects completed follow-up [¹⁸F]MK-6240 scans at six months (6.1 ± 0.5 months), and 16 subjects completed additional follow-up scans at one year (13.3 ± 0.9 months) after the baseline study. Subject characteristics are summarized in Table 1.

Imaging and arterial blood analysis

Subjects underwent T1-weighted (MPRAGE) magnetic resonance (MR) imaging (3 T Magnetom Tim Trio, Siemens Healthineers) and [¹⁸F]MK-6240 PET imaging (180 ± 10 MBq, GE Discovery-MI). Dynamic PET data were collected for 120 min post-injection (6×10 s, 8×15 s, 6×30 s, 8×60 s, 8×120 s, 18×300 s), with an optional 15 min break at 65 min. Computed tomography (CT) scans were acquired for attenuation and scatter corrections. Dynamic PET data were reconstructed using the ordered-subset expectation-maximization algorithm (5 iterations, 16 subsets), including time-of-flight information and point spread function modeling, and were motion-corrected using frame-to-frame realignment (FSL, the FMRIB Software Library).

Table 1. Subject characteristics.

	Age (years)	Sex (M/F)	MMSE	PiB DVR	PiB status	Arterial sampling	6 month follow-up	1 year follow-up	APOE ϵ 4 status	Tau status
CN (n = 24)	68 \pm 12	12M/12F	28 \pm 1	1.5 \pm 0.6	10+/14-	n = 8	n = 20	n = 11	16 APOE ϵ 4-, 6 APOE ϵ 4+, 2 N/A	0+/24-
AD/MCI (n = 8)	70 \pm 11	6M/2F	21 \pm 5	2.3 \pm 0.6	8+/0-	n = 5	n = 5	n = 5	5 APOE ϵ 4-, 3 APOE ϵ 4+	6+/2-

A total of 32 subjects were included in this study. Out of the 32 subjects, eight CN and five AD/MCI subjects had arterial blood sampling at baseline to allow for full quantification with arterial input functions. Twenty-five subjects underwent longitudinal PET scans 6 months after baseline. Out of the 25 subjects, 16 underwent additional longitudinal PET scans 1 year after baseline. No arterial samples were collected at follow-up scans. All values are expressed as mean \pm standard deviation. N/A = data not available.

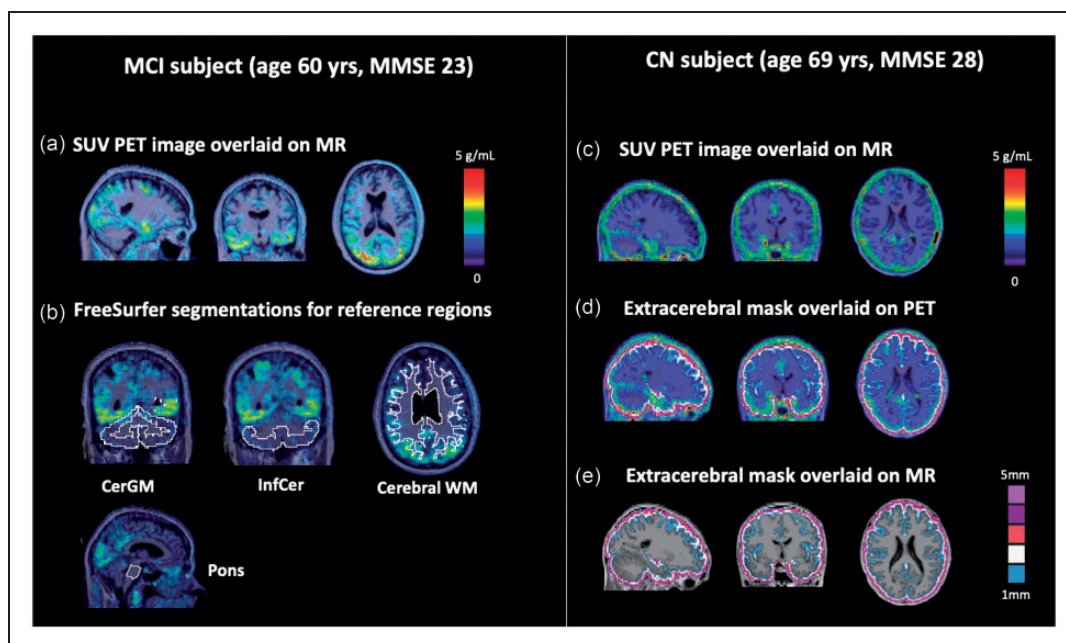


Figure 1. Example [^{18}F]MK-6240 PET images and segmentations for the evaluated reference and extracerebral regions. (a) SUV $_{90-110}$ PET image for a MCI subject (SUV $_{\text{CerGM}} = 2.1$ across target regions) showing characteristic tau uptake pattern in the temporal and occipital lobes. (b) FreeSurfer segmentations of the candidate reference regions overlaid on the SUV $_{90-110}$ image. (c) SUV $_{90-110}$ PET image for a CN subject (SUV $_{\text{CerGM}} = 1.2$ across target regions) showing high extracerebral signal (SUV $_{\text{CerGM}} = 1.4$), especially surrounding the brain hemispheres and the cerebellum. Extracerebral masks overlaid on SUV $_{90-110}$ PET (d) and MR (e) images.

MR images were coregistered to the corresponding PET images (FSL). The PET late-frame uptake (averaged over 90–110 min post-injection) were expressed as standardized uptake values (SUV $_{90-110}$, g/mL). Representative examples are shown in Figure 1(a) and (c).

Arterial blood sampling was performed in 13 subjects (eight CN and five AD/MCI) at baseline to measure whole blood and plasma concentrations of [^{18}F]MK-6240 over the PET scan duration. Details on arterial blood collection and analysis were previously described.⁶ Briefly, arterial samples were collected every 30 s for the first 5 min, then with reduced frequency (15 min) towards the end of the scan. The total

plasma radioactivity was corrected for radiolabeled metabolites of [^{18}F]MK-6240. No arterial blood samples were collected at follow-up visits.

Image processing and regional segmentation

Brain region segmentations were generated using FreeSurfer (version 6).^{27,28} In addition, an extracerebral mask (Figure 1(d) and (e)) was created by dilating the cortical mask by 2–5 mm outward perpendicularly to the cortical surface. Four target regions (entorhinal cortex, amygdala, inferior temporal cortex, and precuneus) were selected for evaluation.

Three types of reference regions were considered (CerGM-based, pons, and cerebral WM-based, Figure 1(b)). To limit spill-in contamination to these regions from the extracerebral signal and cortical regions, voxel erosion was applied. This included erosion of the voxels in the CerGM and WM masks by 1–5 mm from the outer edge (data not shown). Erosion of 3-mm in the CerGM (CerGM_{3mm}) and 4-mm in the WM (WM_{4mm}) were the most appropriate for our tomograph to reduce spill-in signal from extracerebral signal and cortical regions (resulting in no significant difference between the uptake in the AD/MCI and CN groups). The inferior portion of the CerGM (InfCer, Figure 1(b)) was segmented using the spatially unbiased infra-tentorial template (SUIT).²⁹ Voxel counts of the eroded and non-eroded reference region segmentations are listed in Supplementary Table 2. The MR-to-PET transformation matrices were applied to the regional segmentations to enable sampling in PET space and the generation of time-activity curves (TACs).

PET data analyses

In target regions, standardized uptake value ratios ($SUVR = SUV_{\text{target}}/SUV_{\text{reference}}$) were computed to assess tau load, with late-frame measures denoted as $SUVR_{90-110}$. PVC was applied to the non-eroded reference and target regions late-frame uptake data, using the PetSurfer implementation of the symmetric geometric transfer matrix (GTM) algorithm.³⁰

Spectral analysis (SAKE software) was used to evaluate the kinetics of [¹⁸F]MK-6240 in reference and extracerebral regions, as well as the impact of the extracerebral signal on reference region uptake.^{31–35} Spectral analysis decomposed the regional TACs (0–120 min, decay-corrected) into spectral components associated with unique frequency β (min^{-1}) and amplitude α ($\text{mL} \cdot \text{cm}^{-3} \cdot \text{min}^{-1}$), and estimated the $K_{1,SA}$ and $V_{T,SA}$ macro-parameters. Spectral analysis results were used to determine the optimal compartmental configuration (see details in the Supplementary Materials). To evaluate the effect of a shorter scan duration on the amount of extracerebral signal contamination in the reference regions, spectral analysis was repeated using 0–90 min of dynamic data.

Compartmental and graphical analyses were applied to [¹⁸F]MK-6240 PET data acquired with arterial blood samples ($n = 13$). For the reference regions, the total distribution volume (V_T) was estimated using a two-tissue compartmental model (2TCM, $V_{T,2TCM}$) and the Logan graphical method ($V_{T,Logan}$) assuming a fixed blood volume ($V_b = 5\%$, $t^* = 50$ min).³⁶ Measures of tau deposition were based on the distribution volume ratio ($DVR = V_{T,\text{target}}/V_{T,\text{reference}}$). The

non-displaceable binding potential ($BP_{ND} = DVR - 1$) was computed using reference tissue analyses that included the reference Logan ($t^* = 50$ min) and multi-linear reference tissue modeling (MRTM2, $t^* = 30$ min, $k_2' = 0.04$) methods.^{37,38}

Statistical analysis

Baseline SUV_{90-110} , spectral analysis parameters (α and β), and V_T values were compared across reference and extracerebral regions using analysis of variance (ANOVA, to compare group means) and F-test (to compare regional inter-subject variability). Group differences between AD/MCI and CN subjects were evaluated using two-sample T-tests. The SUV_{90-110} with and without PVC were compared using ANOVA and F-test in the candidate reference regions. Linear regression models were used to compare (1) the V_T values estimated using 2TCM, Logan, and spectral analysis and (2) the K_1 values estimated using 2TCM and spectral analysis. Target region DVR and $SUVR_{90-110}$ obtained with the different candidate reference regions were compared using ANOVA and F-test in the AD/MCI and CN groups separately.

The SUV_{90-110} at baseline and longitudinal follow-ups were compared using paired T-tests in the reference and extracerebral regions. Longitudinal changes in SUV_{90-110} ($\Delta SUV_{90-110} = SUV_{90-110, \text{follow-up}} - SUV_{90-110, \text{baseline}}$) were computed at 6-month and 1-year follow-ups, and compared across reference regions using ANOVA and across diagnostic groups using unpaired T-test.

Subjects ($n = 32$) were classified into a binary group (high/low) based on their baseline extracerebral $SUVR_{90-110}$ (CerGM_{3mm} reference region). The binary classification was obtained using histogram analysis and subsequently verified by k-means clustering ($k = 2$), and a threshold for classification as high/low extracerebral signal was calculated.

Bonferroni corrections were applied for all statistical comparisons, with significance assessed at $p = 0.05$.

Group outcome measures were expressed as mean \pm standard deviation. Inter-subject variability was defined as the standard deviation of a group outcome measure. Kolmogorov-Smirnov test was used to examine the normality of the SUV_{90-110} and V_T values in all subjects, and $SUVR_{90-110}$ and DVR values in the AD/MCI and CN groups separately.

Effect size estimation

To further inform the impact of reference region selection on target region outcomes, we performed effect size estimations using the different candidate reference regions for:

- a. Cross sectional data: differentiating target region SUV_{90-110} between 1) AD/MCI and CN, and 2) $A\beta+$ and $A\beta-$ individuals, as another hallmark pathology of AD with a crucial role preceding tau accumulation and cognitive decline.³⁹⁻⁴¹
- b. Longitudinal data: detecting annual changes (one year after baseline) in target region SUV_{90-110} in 1) AD/MCI, and 2) $A\beta+$ individuals.

Effect sizes were estimated using Hedge's g coefficients (see details in the Supplementary Materials). Similar effect size estimations were performed using DVR (MRTM2) as the target region outcomes.

Criteria for selection of the preferred reference region

The following criteria were evaluated (ranked in order of importance):

1. Negligible tissue concentrations of neurofibrillary tangles of tau
2. Low spill-in contamination from adjacent regions with high specific (e.g., target) and/or nonspecific (e.g., extracerebral) uptake
3. Low longitudinal variability in uptake measures
4. Consistent uptake characteristics across diagnostic groups to limit the impact of reference region on target region outcomes (i.e., low inter-subject variability across AD/MCI and CN subjects)

Ethics approval. All procedures performed in studies involving human participants were in accordance with the ethical standards of the institutional and/or national research committee and with the 1964 Helsinki Declaration and its later amendments or comparable ethical standards.

Consent to participate. Written consents were obtained from all participants.

Results

Baseline SUV_{90-110} in the reference and extracerebral regions

Example SUV images and TACs are shown for an MCI (Figures 1(a) and 2(a)) and a CN (Figures 1(c) and 2(b)) subject. The pons SUV_{90-110} (0.31 ± 0.08) was significantly lower in magnitude and inter-subject variability compared to other candidate reference regions (Table 2, Figure 2(c)). The InfCer SUV_{90-110} (0.64 ± 0.14) showed the highest magnitude among all candidate reference regions. No significant differences in SUV_{90-110} were observed across other candidate

reference regions. Applying PVC or erosion to the SUV_{90-110} data slightly reduced the SUV_{90-110} magnitudes in WM and CerGM compared to the non-PVC and non-eroded data (not significant) (Supplementary Table 3). Applying PVC increased the SUV_{90-110} inter-subject variability by 16–60% in reference regions. The rank order of the SUV_{90-110} magnitudes was consistent with and without PVC.

The WM SUV_{90-110} was the only candidate reference region where the SUV_{90-110} was significantly higher in the AD/MCI than the CN group. Applying erosion of at least 4-mm or PVC reduced the group differences in WM SUV_{90-110} (not significant).

The extracerebral SUV_{90-110} (0.78 ± 0.16) showed significantly higher magnitude but similar inter-subject variability than the candidate reference regions SUV_{90-110} . No significant group differences were observed in the extracerebral SUV_{90-110} .

Spectral analysis in the reference and extracerebral regions

Spectral analysis identified two reversible components and one trapping component in all candidate reference regions, and identified one reversible component and one trapping component in the extracerebral signal (Figure 3(a) and (b)).

The first reversible component ($\beta \sim 0.18 \text{ min}^{-1}$, faster kinetics, Figure 3(c)) likely reflects radiotracer delivery. No significant differences in β values were observed between the reference and extracerebral regions. The α values in the CerGM-based regions ($\sim 0.49 \text{ mL} \cdot \text{cm}^{-3} \cdot \text{min}^{-1}$) were significantly higher than in WM and pons ($\sim 0.23 \text{ mL} \cdot \text{cm}^{-3} \cdot \text{min}^{-1}$). The α values in the extracerebral signal ($0.05 \text{ mL} \cdot \text{cm}^{-3} \cdot \text{min}^{-1}$) were significantly lower than in all reference regions.

The second reversible component ($\beta \sim 0.03 \text{ min}^{-1}$, slower kinetics, Figure 3(d)) likely captures the late-frame uptake. No significant differences in β values were observed between the candidate reference regions, whereas α values in the WM and pons ($\sim 0.05 \text{ mL} \cdot \text{cm}^{-3} \cdot \text{min}^{-1}$) were slightly higher than in the CerGM-based regions ($\sim 0.10 \text{ mL} \cdot \text{cm}^{-3} \cdot \text{min}^{-1}$, not significant). The extracerebral signal did not exhibit this component.

A trapping component ($\beta = 10^{-5} \text{ min}^{-1}$, Figure 3(e)) was present in all candidate reference and extracerebral regions, likely reflecting irreversible uptake. The α values in the extracerebral signal ($0.03 \text{ mL} \cdot \text{cm}^{-3} \cdot \text{min}^{-1}$) were 2.5-fold higher than in all candidate reference regions. Compared to the CerGM ($0.01 \text{ mL} \cdot \text{cm}^{-3} \cdot \text{min}^{-1}$), the α values were lower in WM and pons ($0.006 \text{ mL} \cdot \text{cm}^{-3} \cdot \text{min}^{-1}$) and higher in InfCer ($0.02 \text{ mL} \cdot \text{cm}^{-3} \cdot \text{min}^{-1}$). Applying erosion to the

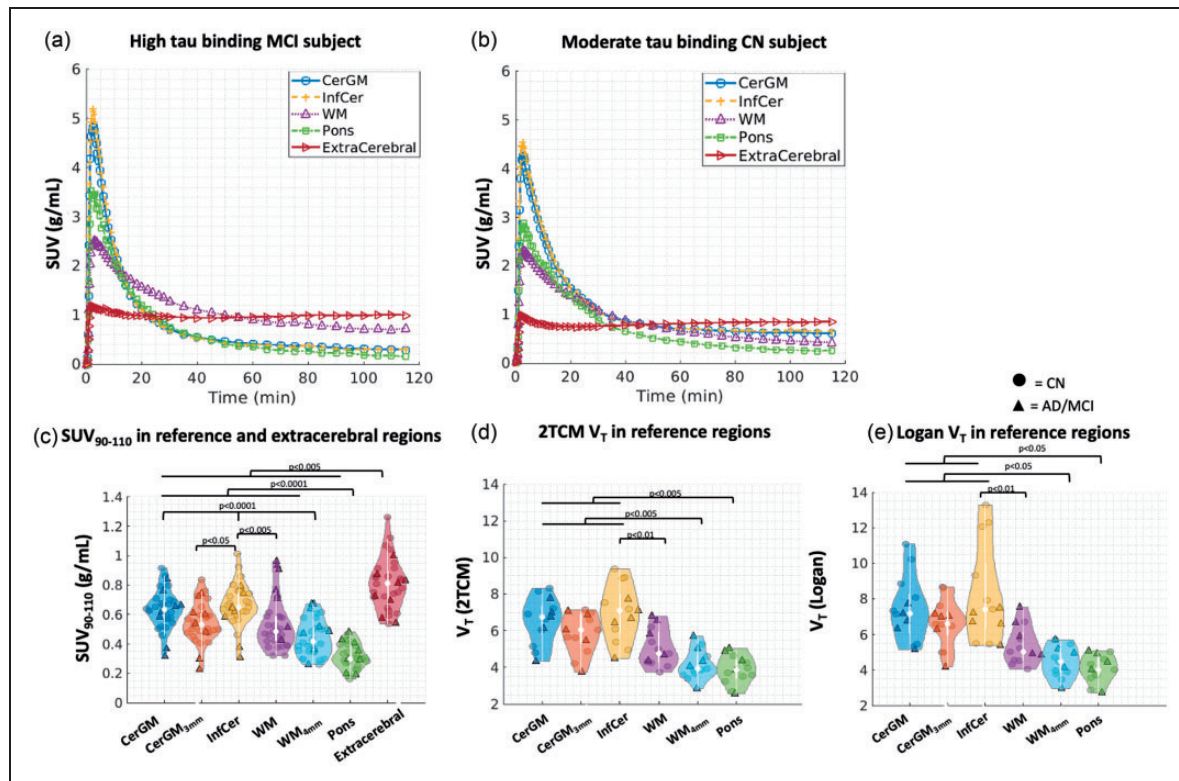


Figure 2. Time-activity characteristics and V_T in the candidate reference regions and the extracerebral region. Time-activity curves were shown for a high tau binding MCI subject (a) and a CN subject (b) in the CerGM, InfCer, WM, pons, and extracerebral regions (data points were connected using linear interpolation). (c) The SUV_{90-110} in the reference and extracerebral regions ($n = 32$), showing the lowest SUV_{90-110} in the pons and the highest SUV_{90-110} in the InfCer among all candidate reference regions. The V_T values ($n = 13$) estimated using 2TCM (d) and Logan graphical analysis (e) were also the lowest in the pons and the highest in the InfCer.

CerGM and WM reduced the α values by 25% compared to the non-eroded data.

No significant differences in the α nor β values were observed between the CN and AD/MCI groups in any non-target region. Spectral analysis results obtained using 90 min and 120 min of dynamic data were consistent.

Compartmental and graphical analyses in the reference regions

The V_T in pons and WM_{4mm} showed significantly lower magnitudes than in CerGM-based regions, and significantly lower inter-subject variability than in InfCer (Table 2, Figure 2(d) and (e)). No significant differences in V_T magnitudes and variability were observed across other reference regions. No significant differences between diagnostic groups were observed in any reference region. Eroding the CerGM and WM slightly reduced the V_T magnitudes (not significant). Both 2TCM and Logan graphical methods failed to model the extracerebral uptake.

The V_{T_Logan} and V_{T_2TCM} values correlated significantly in all candidate reference regions ($p < 10^{-5}$).

Compared to V_{T_2TCM} , V_{T_Logan} values showed the highest positive bias in the InfCer (25%) and lowest in the pons and WM (8%). Eroding the CerGM reduced the bias by 15%. The V_{T_SA} and V_{T_2TCM} values correlated significantly in the pons and WM ($p < 0.05$, slope: 0.7–1.0) but not in CerGM-based regions. The K_{1_SA} and K_{1_2TCM} values correlated significantly in all candidate reference regions ($p < 10^{-6}$) with less than 3% bias.

Longitudinal changes (ΔSUV_{90-110}) in reference and extracerebral uptake

At group level, none of the candidate reference regions showed significant ΔSUV_{90-110} at either the 6-month or 1-year follow-up (Table 2, Figure 4). The ΔSUV_{90-110} magnitudes were similar between diagnostic groups and were lowest in the pons (6-month: 0.02 ± 0.05 , 1-year: -0.002 ± 0.07) and highest in the CerGM-based regions (6-month: 0.04 ± 0.07 , 1-year: 0.04 ± 0.13 , Supplementary Table 3), although no statistically significant differences were observed across reference regions. The ΔSUV_{90-110} in candidate reference regions showed high inter-subject (range: 0.05–0.13) and

Table 2. The SUV₉₀₋₁₁₀ (baseline and follow-ups) and V_T (baseline) values in the reference and extracerebral regions.

	SUV ₉₀₋₁₁₀					
	Baseline (n = 32)		6-month (n = 25)		1-year (n = 16)	
	CN (n = 24)	AD/MCI (n = 8)	CN (n = 20)	AD/MCI (n = 5)	CN (n = 11)	AD/MCI (n = 5)
CerGM	0.62 ± 0.12	0.59 ± 0.17	0.67 ± 0.18	0.65 ± 0.20	0.71 ± 0.14	0.58 ± 0.13
CerGM _{3mm}	0.53 ± 0.13	0.51 ± 0.17	0.59 ± 0.19	0.56 ± 0.20	0.64 ± 0.13	0.50 ± 0.14
InfCer	0.66 ± 0.13	0.57 ± 0.16	0.71 ± 0.18	0.64 ± 0.19	0.77 ± 0.13	0.58 ± 0.15
WM	0.44 ± 0.10 ^a	0.73 ± 0.20 ^a	0.48 ± 0.13 ^a	0.90 ± 0.21 ^a	0.52 ± 0.11 ^a	0.80 ± 0.15 ^a
WM _{4mm}	0.42 ± 0.11	0.51 ± 0.15	0.43 ± 0.10	0.55 ± 0.13	0.48 ± 0.13	0.46 ± 0.03
Pons	0.30 ^b ± 0.08 ^c	0.32 ^b ± 0.09 ^c	0.30 ^b ± 0.10 ^c	0.34 ^b ± 0.10 ^c	0.31 ^b ± 0.07 ^c	0.28 ^b ± 0.03 ^c
Extracerebral	0.78 ^b ± 0.15	0.74 ^b ± 0.17	0.85 ^b ± 0.18	0.81 ^b ± 0.17	0.79 ^b ± 0.17	0.83 ^b ± 0.21

	Baseline (n = 13) with arterial sampling					
	V _T 2TCM		V _T Logan		V _T SA	
	CN (n = 8)	AD/MCI (n = 5)	CN (n = 8)	AD/MCI (n = 5)	CN (n = 8)	AD/MCI (n = 5)
CerGM	6.66 ± 1.29	6.39 ± 1.29	7.94 ± 2.08	6.62 ± 0.98	4.32 ± 0.83	6.18 ± 2.14
CerGM _{3mm}	5.88 ± 1.03	5.88 ± 1.34	6.81 ± 1.43	6.31 ± 1.25	4.76 ± 1.07	6.38 ± 2.01
InfCer	7.28 ± 1.69	6.48 ± 1.21	9.16 ± 3.09 ^c	6.69 ± 0.81 ^c	4.37 ± 1.13	6.78 ± 2.48
WM	4.71 ± 0.80	5.63 ± 1.09	5.02 ± 0.87	5.97 ± 1.16	3.90 ± 0.70	4.80 ± 1.33
WM _{4mm}	4.01 ^b ± 0.62	4.39 ^b ± 1.08	4.42 ^b ± 0.81	4.58 ^b ± 1.06	4.01 ^b ± 1.00	4.19 ^b ± 1.39
Pons	3.69 ^b ± 0.61	4.14 ^b ± 0.99	3.98 ^b ± 0.66	4.23 ^b ± 0.94	4.33 ^b ± 1.65	4.29 ^b ± 1.17

All values are expressed as mean ± standard deviation.

^aSignificantly different between the CN and AD/MCI groups.

^bMean magnitudes were significantly different compared to the CerGM.

^cStandard deviations were significantly different compared to the CerGM.

intra-subject (range: -0.24–0.26) variability at both follow-ups. Eroding the CerGM and WM did not impact the magnitude nor variability of Δ SUV₉₀₋₁₁₀ measures. Applying PVC did not impact the magnitude but significantly increased the inter- and intra-subject variability of Δ SUV₉₀₋₁₁₀ measures. At group level, the extracerebral Δ SUV₉₀₋₁₁₀ (6-month: 0.01 ± 0.12, 1-year: 0.0002 ± 0.16) was similar across diagnostic groups, with similar magnitudes but higher inter-subject variability than the reference regions Δ SUV₉₀₋₁₁₀.

Target region uptake quantification

The target region DVR and SUVR₉₀₋₁₁₀ values were significantly higher in the AD/MCI group than in the CN group, for all candidate reference regions ($p < 0.001$) except for the non-eroded WM.

In the CN group, the target region DVR and SUVR₉₀₋₁₁₀ showed higher magnitude and inter-subject variability using the pons or WM as reference regions, compared to CerGM-based reference regions ($p < 0.05$, Figure 5(a), Supplementary Table 4). Eroding the CerGM or WM slightly increased the target region DVR and SUVR₉₀₋₁₁₀ magnitudes (not significant) without affecting the variability.

In the AD/MCI group, the SUVR₉₀₋₁₁₀ and DVR values using WM reference region showed the lowest magnitude and variability (not significant, Figure 5(b), Supplementary Table 4). The target region SUVR₉₀₋₁₁₀ and DVR values using pons and eroded WM as reference regions showed the highest magnitude and variability compared to using CerGM reference region (not significant, Supplementary Fig.1).

Applying PVC to the reference and target region SUVR₉₀₋₁₁₀ data showed consistent SUVR₉₀₋₁₁₀ magnitude rank orders across candidate reference regions, but a 2-fold increase in inter-subject variability compared to the non-PVC data (in both CN and AD/MCI groups).

Effect size estimation

For differentiating between subject groups in cross-sectional SUVR₉₀₋₁₁₀ data, the use of the CerGM_{3mm} as reference region resulted in the largest effect size (1.14–1.55 for AD/MCI vs. CN; 0.72–1.19 for A β + vs A β - groups), although we found no significant differences between the CerGM-based reference regions. The WM showed the lowest effect size (-0.04–0.86 for AD/MCI vs. CN; 0.18–0.45 for A β + vs A β - groups).

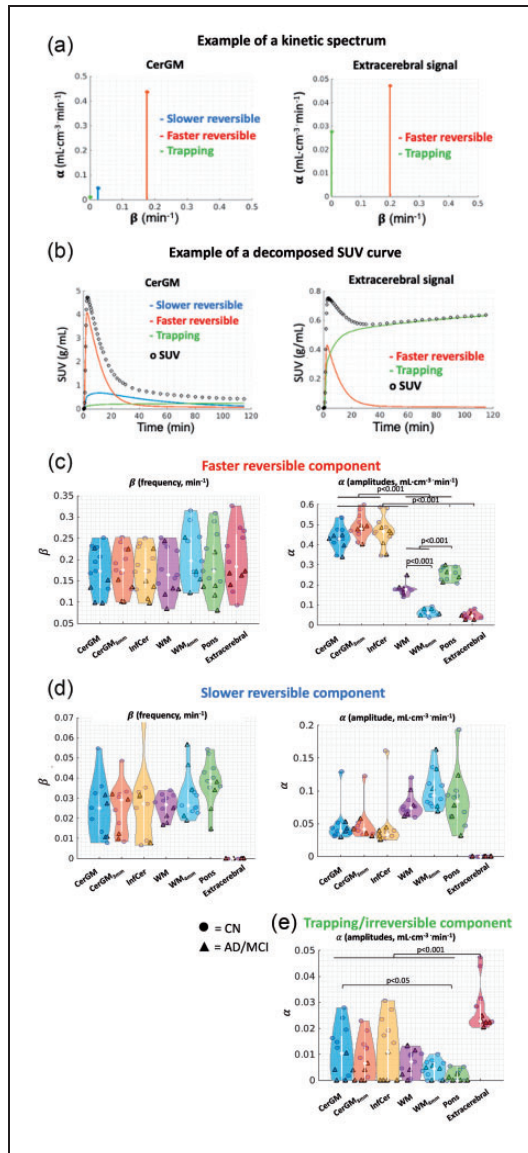


Figure 3. Spectral analysis results in the candidate reference regions and extracerebral region. Examples of (a) kinetic spectrum and (b) decomposed time-activity curve in the reference and extracerebral region. (c) Along the faster reversible component, no significant difference in the β values was observed. The α values were the highest in the CerGM-based reference regions, followed by the WM and pons, and the lowest in the WM_{4mm} and extracerebral signal. (d) Along the slower reversible component, no significant differences in the α nor β values were observed between the candidate reference regions. The extracerebral signal did not exhibit the slower reversible component. (e) Along the trapping component ($\beta = 10^{-5} \text{ min}^{-1}$), the α values in the extracerebral signal were higher than all candidate reference regions. The α values were highest in the CerGM-based regions, followed by WM, and lowest in the pons. The units of α and β values were min^{-1} and $\text{mL}\cdot\text{cm}^{-3}\cdot\text{min}^{-1}$, respectively.

Among the examined target regions, the effect size was the largest in the amygdala, followed by the entorhinal, and lowest in the inferior temporal and precuneus (Supplementary Table 5).

For detecting longitudinal change over a one-year period in target region SUVR_{90-110} , the effect size was not statistically significant in our sample (i.e., the 95% confidence interval contains zero). Our preliminary longitudinal effect size estimation suggested that the effect size was highest using the pons as reference region, followed by eroded WM_{4mm}, and was lowest in the CerGM-based regions in the AD/MCI group (Supplementary Table 6). However no statistically significant differences were found between reference regions. Similar results were obtained in the $\text{A}\beta+$ group.

Using DVR values as target region outcomes resulted in similar effect sizes as with SUVR_{90-110} .

Extracerebral signal threshold

Using histogram analysis, an extracerebral SUVR_{90-110} threshold of 1.29 that assigned 50% of subjects to a high extracerebral uptake group was obtained (Supplementary Fig.2ab, Supplementary Table 7). No significant difference in extracerebral SUVR_{90-110} between the CN and AD/MCI groups was observed. No significant correlations between the extracerebral SUVR_{90-110} and clinical characteristics (i.e., age, PiB DVR, MMSE, sex) were observed. The group assignments remained unchanged for all subjects at both follow-ups except for one MCI subject who changed from the low to the high extracerebral group at the one-year follow-up.

Discussion

In this study, we examined the kinetics of the [¹⁸F]MK-6240 uptake signal in the extracerebral region and in alternative reference regions potentially less prone to extracerebral contamination signal than CerGM. We also evaluated the impact of these reference regions on target region uptake. Among the candidate reference regions, the pons and WM_{4mm} showed lowest inter-subject variability in SUV_{90-110} and V_T , lowest longitudinal change in SUV_{90-110} , lowest contamination from the extracerebral signal, highest dynamic range of target region uptake in both the CN and AD/MCI groups. In cross-sectional studies, CerGM-based reference regions resulted in the largest effect sizes for differentiating participant groups (AD/MCI and CN; $\text{A}\beta+$ and $\text{A}\beta-$). When considering

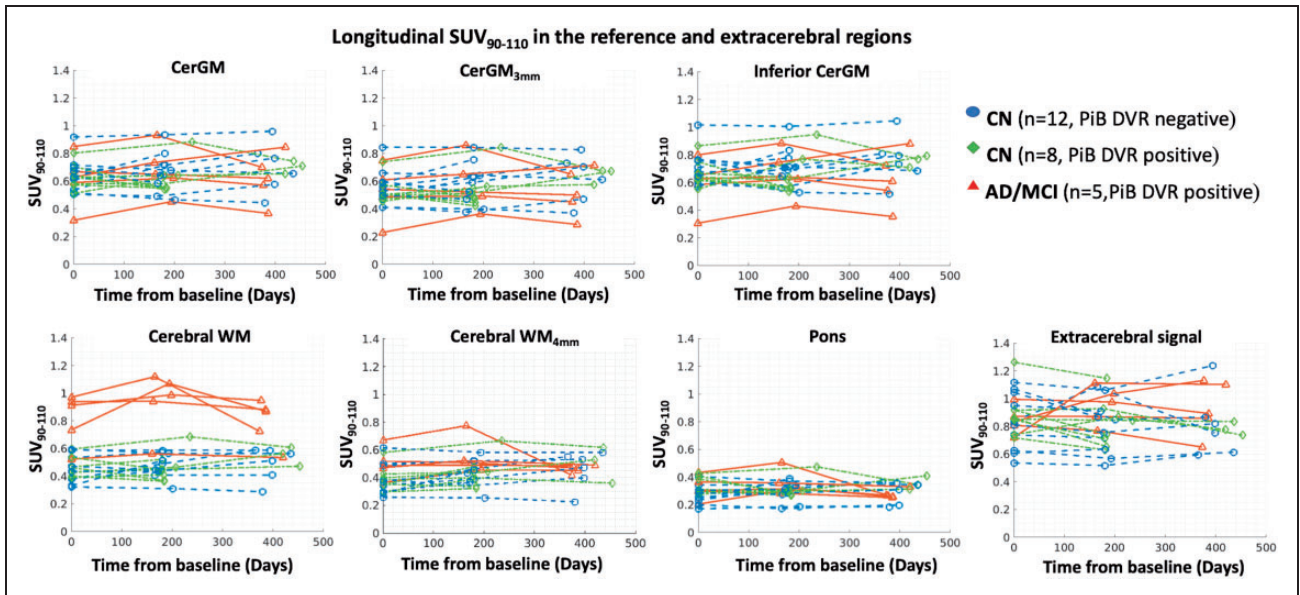


Figure 4. The longitudinal changes of $SUVR_{90-110}$ in the candidate reference regions and the extracerebral region at baseline, 6-month, and 1-year follow-ups (the x-axis indicates the days after the baseline PET scans). No significant longitudinal change in $SUVR_{90-110}$ was observed over 1-year in any reference or extracerebral region at the group level.

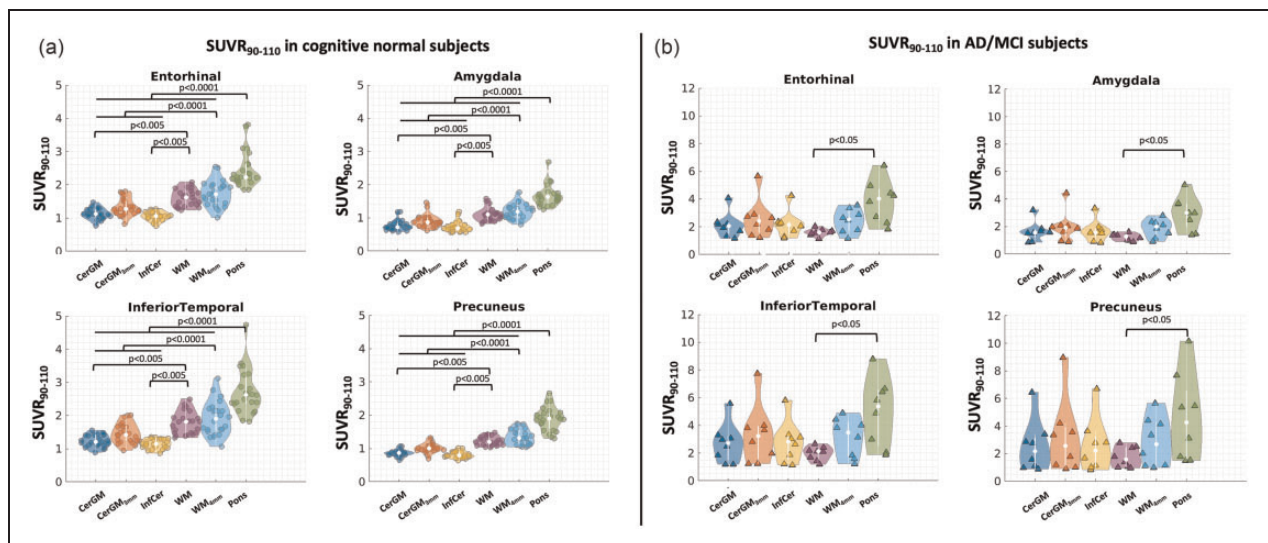


Figure 5. Target region $SUVR_{90-110}$ (in the entorhinal, amygdala, inferior temporal, and precuneus) using each candidate reference region. (a) In the CN group, target region $SUVR_{90-110}$ using the pons, WM, and eroded WM as the reference region were significantly higher than those using the CerGM-based reference regions. (b) In the AD/MCI group, target region $SUVR_{90-110}$ using the pons as the reference region were significantly higher than those using the WM as the reference region.

Spectral analysis

CerGM-based reference regions, our results highlighted the necessity of eroding from both the inferior and superior directions to limit contamination from the extracerebral signal.

Spectral analysis was used to evaluate the tracer kinetics without assumptions about the kinetic compartment configuration. Our results support a reversible two-tissue compartmental configuration in the reference

regions, consistent with previous studies that found that the two-tissue compartmental model was preferred over the one-tissue in the CerGM and pons.^{2,6} Spectral analysis provided two reversible components in all candidate reference regions. The first reversible component likely reflects radiotracer delivery. We found lower α values in the WM and pons compared to CerGM-based regions, consistent with the lower peak magnitudes in the TACs (Figure 2(a) and (b)). In addition, the α values of this component correlated significantly with the K_{1-2TCM} values, confirming that this faster component reflects radiotracer delivery. The second reversible component likely captures the late-frame characteristics and may reflect non-specific binding in reference regions. The higher α values (reflecting the slower kinetics) in the WM and pons were consistent with their lower SUV_{90-110} compared to CerGM-based regions. All candidate reference regions showed various levels of the trapping component (likely reflecting irreversible binding), which may represent the level of off-target or extracerebral signal contamination. The spectral analysis accurately estimated the radiotracer delivery (K_1) values; however, the $V_{T,SA}$ values only agreed with the $V_{T,2TCM}$ in regions with low trapping component (i.e., pons, WM, and WM_{4mm}). These discrepancies may be attributed to the differences in the two methods: the calculation of $V_{T,SA}$ does not include the trapping component, while 2TCM assumes no trapping/irreversible binding.

The kinetics of the extracerebral signal appeared different from the reference regions, with lower peaks in the TACs and increased uptake in late frames (Figure 2 (a) and (b)), as also reported in another study.² We showed that the extracerebral signal exhibited a single reversible component and a high contribution of the trapping component. The lower α values of the faster reversible component were consistent with the lower peaks in the extracerebral TACs compared to candidate reference regions, and suggest that the extracerebral signal is less prominent in early-frame data. The high α values of the trapping component suggest that the irreversible uptake behavior of the extracerebral signal was dominant in the late frame data. Since no irreversible uptake is expected in reference region, the α values of the trapping component likely reflected the level of off-target or extracerebral signal contamination. The WM and pons were protected from the extracerebral signal contamination due to their anatomical locations, whilst the CerGM and InfCer, the most used reference regions in the current [¹⁸F]MK-6240 literature, were most vulnerable. Eroding the CerGM from the outer edge voxels reduced the signal contamination from the extracerebral and cortical regions, emphasizing the importance of eroding from

both the inferior and superior sides. Several studies attempted to reduce extracerebral signal contamination by shortening scan durations (e.g. 70–90 min).^{2,9,11,15} However, our results suggested that this does not significantly reduce extracerebral signal contamination (estimated by the trapping component). A longer scan duration (up to 120 min) may be preferred as the target region uptake in high binding subjects may not have reached adequate equilibrium at 90 min.

Reference region uptake quantification

The WM showed significantly higher SUV_{90-110} in the AD/MCI than the CN group, suggesting the presence of specific tau uptake in the AD/MCI group, likely due to spill-in from neighboring high uptake regions. Previous studies suggested that using the WM as reference region significantly increased statistical power for detecting within-subject longitudinal changes of target region uptake compared to CerGM-based reference regions.^{19,42} This is likely because the WM showed lower SUV_{90-110} magnitude (hence generating a higher dynamic range in target region uptake) and has a larger size than the CerGM-based reference regions. However, the spill-in of specific tau uptake to the WM can reduce the sensitivity for detecting group differences in cross-sectional studies involving high binding subjects and for detecting longitudinal changes in target region uptake. Our results showed that eroding the WM by 4mm sufficiently reduced the spill-in signal without increasing the inter-subject variability of the reference region uptake while maintaining a high voxel count.

Among all candidate reference regions, the $V_{T,Logan}$ values showed higher positive bias than $V_{T,2TCM}$ in regions that were more prone to extracerebral signal contamination (i.e., the non-eroded CerGM and InfCer). The InfCer showed the highest V_T inter-subject variability, likely due to the high extracerebral signal contamination from the inferior side of the cerebellum. The SUV_{90-110} inter-subject variability was lower in the pons and WM_{4mm} than in the CerGM-based regions, reducing the impact of reference region variability on target region outcomes. The low uptake in the pons resulted in target region DVR and $SUVR_{90-110}$ values with higher magnitudes than CerGM reference regions in both the CN and AD/MCI groups. Higher dynamic range in target region outcomes may allow for higher sensitivity for detecting tau deposition in early disease or before symptoms onset.⁷

Applying PVC using the GTM method to the SUV_{90-110} data increased the inter-subject variability in all reference regions except the WM. A recent

study evaluated the performance of different PVC methods to reduce the spill-in effects of extracerebral signal into the cortical regions¹⁸ and demonstrated that applying PVC using the region-based voxel wise (RBV) method significantly improved group differences in target region SUVR measures between the CN and MCI groups. More studies are needed to examine the impact of RBV PVC method on the variability of reference region uptake and how that translates to target region uptake in our dataset.

Effect size estimation

Our effect size calculations suggest that CerGM_{3mm} may be the optimal reference region for differentiating between participant groups (AD/MCI vs. CN; A β + vs. A β -) in cross-sectional [¹⁸F]MK-6240 studies, although we did not find significant differences among the CerGM-based regions. The effect size was the largest in the amygdala, followed by the entorhinal, and lowest in the inferior temporal and precuneus, consistent with the rank order in a large, recent [¹⁸F]MK-6240 study⁴³ with a total of 464 subjects (266 CN, 112 MCI and 86 AD). Our effect size calculations failed to detect statistically significant longitudinal changes in the target regions, possibly due to the small sample size available for longitudinal evaluations ($n=5$ in the AD/MCI group; $n=8$ in the A β + group), and the limited longitudinal time points (i.e., one year after baseline). The longitudinal effect size was the highest (borderline significant) when using the pons as reference region. No statistically significant differences were observed between effect size estimations for SUVR₉₀₋₁₁₀ and DVR, suggesting that dynamic acquisition may not improve the detection of group differences nor of longitudinal changes in our limited sample size and longitudinal time points. More subjects are currently enrolling in our study to further validate these findings.

Longitudinal changes in the reference regions

No significant longitudinal SUVR₉₀₋₁₁₀ changes were observed in any of the candidate reference regions, suggesting relatively stable uptake over one year at the group level. A previous study suggested an annual increase of 0.01–0.15 in target region SUVR₉₀₋₁₁₀ across CN and AD subjects.⁴⁴ Our results showed that the longitudinal changes in reference region uptake were similar in both magnitude and variability to the annual increase reported for target region uptake in the CN subjects,⁴⁴ highlighting the importance of evaluating the reference region characteristics, especially in low binding subjects. Among the candidate reference regions, the pons showed slightly lower magnitude

and variability of the change measure, and may be preferred as the reference region used for longitudinal studies. These preferred longitudinal characteristics may contribute to the highest longitudinal effect size when using the pons as reference region compared to the CerGM-based regions. A divergence in the optimal reference region selection between cross-sectional and longitudinal studies is possible, as has also been shown for first-generation tau and A β radiotracers: while CerGM-based reference regions may be preferred for cross-sectional studies, WM-rich regions may be preferred for longitudinal studies.^{19,45,46}

Erosion of the outer voxels of the CerGM and WM slightly decreased the variability of the change measures compared to the non-eroded data, likely due to the reduction of spill-in contamination signal. Applying PVC to reference region uptake significantly increased the variability of the change measures compared to the non-PVC data, which may be detrimental for the robust estimation of longitudinal changes in target region uptake. More studies are needed to examine the performance of different PVC methods (e.g., RBV) on longitudinal changes in target region uptake.

Extracerebral uptake quantification and longitudinal changes

In our study, 50% of subjects showed high extracerebral uptake, consistent with a recent study.¹⁸ Another recent study suggested a sex-related effect in the extracerebral uptake;¹⁷ we didn't observe a sex-related difference in extracerebral uptake, which may be due to the smaller sample size in our study. The heterogeneous nature of the extracerebral signal may impact the accurate quantification of tau uptake in both the target (e.g., inferior temporal and entorhinal cortex) and reference (e.g., CerGM and InfCer) regions. The extracerebral uptake was stable over one year at the group level but exhibited high inter- and intra-subject variability, independent of the diagnostic group. The variable nature of the extracerebral signal across subjects should be considered, and either erosion or PVC should be applied, especially in cross-sectional studies involving low binding subjects and in longitudinal studies.

Limitations

The limitations in this study include a relatively small number of participants with arterial blood samples. The V_{T_2TCM} values in this study were comparable with previous studies, and the rank orders of reference region uptake estimated by V_T and SUVR₉₀₋₁₁₀ were consistent in all candidate reference regions.^{6,8} Our study focused primarily on CN subjects;

the small number of AD/MCI subjects limited the statistical power for examining group differences in reference and target region uptake. Similarly, our sample size may not allow accurate estimation of effect sizes, especially for detecting longitudinal changes in target regions over one year. The lack of test-retest data prevents us from determining the test-retest variability of reference region uptake and from comparing the test-retest variability to the longitudinal changes of reference region uptake. Further investigations are needed to evaluate the test-retest variability of reference region uptake. In this study, we quantified the unique kinetics of the extracerebral signal. Additional studies are needed to explore methods for correcting for the extracerebral signal contamination in both target and reference regions without introducing additional variability. The unique kinetic spectra of the extracerebral signal could potentially be leveraged for removing the trapping component from the time-activity data in subjects with high extracerebral signal.

In summary, our results suggested that careful considerations should be taken in the selection of optimal reference regions for [^{18}F]MK-6240 studies. The most used reference regions in the current literature (CerGM and InfCer) still present a considerable level of extracerebral signal contamination that can result in high inter-subject variability in reference region uptake and influence longitudinal change measures. Among the examined reference regions, the pons and WM_{4mm} may be preferred for longitudinal [^{18}F]MK-6240 studies due to their low inter-subject variability and low magnitude in uptake, low variability in longitudinal change, and low level of extracerebral signal contamination. However, effect size calculations suggest that the CerGM-based regions may be the optimal reference region for differentiating between participant groups (AD/MCI vs. CN; A β + vs. A β -) in cross-sectional [^{18}F]MK-6240 studies. We also showed that when using CerGM reference regions, eroding from both the inferior and superior sides may be necessary to account for extracerebral signal contamination. Even though the physiological nature of the extracerebral signal is not yet understood, our results suggested that the extracerebral signal is stable over time at the group level. However, efforts should be made to correct the extracerebral signal contamination due to its high inter- and intra-subject variability.

Funding

The author(s) disclosed receipt of the following financial support for the research, authorship, and/or publication of this article: This work is supported by the following grants: NIH R01AG046396, R01AG050436, R01AG052414, S10OD018035, P41EB022544, T32EB013180 and R01AG076153.

Acknowledgements

The authors thank Mattia Veronese for sharing the spectral analysis codes.

Declaration of conflicting interests

The author(s) declared no potential conflicts of interest with respect to the research, authorship, and/or publication of this article.

Authors' contributions

JFF: data processing, data analysis, figure generation, results interpretation, manuscript preparation (draft and edit).

CL: data processing, data analysis, results interpretation, manuscript preparation (draft and edit).

JS: data processing, data collection, data analysis, provide critical feedback on manuscript.

JAB: data processing, data analysis, provide critical feedback on manuscript.

ZBR: data processing, data collection.

ET: data processing, data collection.

ANS: data processing, provide critical feedback on manuscript.

HS: data processing, provide critical feedback on manuscript.

MEF: data processing, provide critical feedback on manuscript.

NJG: data processing, results interpretation, provide critical feedback on manuscript.


MDN: data processing, results interpretation, provide critical feedback on manuscript.

GEF: study design, results interpretation, provide critical feedback on manuscript.

KAJ: study design, results interpretation, provide critical feedback on manuscript.

JCP: study design, results interpretation, manuscript preparation (edit).

ORCID iD

Jessie Fanglu Fu  <https://orcid.org/0000-0002-4970-7811>

Supplementary material

Supplemental material for this article is available online.

References

- Walji AM, Hostetler ED, Selnick H, et al. Discovery of 6-(fluoro-18F)-3-(1H-pyrrolo[2,3-c]pyridin-1-yl)isoquinolin-5-amine ([^{18}F]-MK-6240). A positron emission tomography (PET) imaging agent for quantification of neurofibrillary tangles (NFTs). *J Med Chem* 2016; 59: 4778–4789.
- Bethausen TJ, Cody KA, Zammit MD, et al. In vivo characterization and quantification of neurofibrillary tau PET radioligand 18F-MK-6240 in humans from Alzheimer disease dementia to young controls. *J Nucl Med* 2019; 60: 93–99.
- Lois C, Gonzalez I, Johnson KA, et al. PET imaging of tau protein targets: a methodology perspective. *Brain Imaging Behav* 2019; 13: 333–344.

4. Pascoal TA, Shin M, Kang MS, et al. In vivo quantification of neurofibrillary tangles with [18F]MK-6240. *Alzheimer's Res Ther* 2018; 10: 74.
5. Aguero C, Dhaynaut M, Normandin MD, et al. Autoradiography validation of novel tau PET tracer [F-18]-MK-6240 on human postmortem brain tissue. *Acta Neuropathol Commun* 2019; 7: 37.
6. Guehl NJ, Wooten DW, Yokell DL, et al. Evaluation of pharmacokinetic modeling strategies for in-vivo quantification of tau with the radiotracer [18F]MK6240 in human subjects. *Eur J Nucl Med Mol Imaging* 2019; 46: 2099–2111.
7. Betthauser TJ, Kosciak RL, Jonaitis EM, et al. Amyloid and tau imaging biomarkers explain cognitive decline from late middle-age. *Brain* 2020; 143: 320–335.
8. Salinas C, Lohith TG, Purohit A, et al. Test–retest characteristic of [18F]MK-6240 quantitative outcomes in cognitively normal adults and subjects with Alzheimer's disease. *J Cereb Blood Flow Metab* 2020; 40: 2179–2187.
9. Betthauser TJ, Kosciak RL, Jonaitis EM, et al. MK-6240 imaging features, cognitive associations in preclinical Alzheimer's disease and a case with imaging-to-postmortem correlates. *Alzheimer's Dement* 2020; 16: e043217.
10. Pascoal TA, Therriault J, Benedet AL, et al. 18F-MK-6240 PET for early and late detection of neurofibrillary tangles. *Brain* 2020; 143: 2818–2830.
11. Lohith TG, Bennacef I, Vandenberghe R, et al. Brain imaging of Alzheimer dementia patients and elderly controls with 18 F-MK-6240, a PET tracer targeting neurofibrillary tangles. *J Nucl Med* 2019; 60: 107–114.
12. Pascoal TA, Therriault J, Benedet AL, et al. 18F-MK-6240 PET for early and late detection of neurofibrillary tangles. *Brain* 2020; 143: 2818–2830.
13. Therriault J, Pascoal TA, Benedet AL, et al. Frequency of biologically defined Alzheimer disease in relation to age, sex, APOE ε4, and cognitive impairment. *Neurology* 2021; 96: e975–e985.
14. Pascoal TA, Benedet AL, Ashton NJ, et al. Microglial activation and tau propagate jointly across braak stages. *Nat Med. Epub* 2021; ahead of print. DOI:10.1038/s41591-021-01456-w.
15. Gogola A, Minhas DS, Villemagne VL, et al. Direct comparison of the tau PET tracers [18 F]flortaucipir and [18 F]MK-6240 in human subjects. *J Nucl Med* 2022; 63: 108–116.
16. Leuzy A, Pascoal TA, Strandberg O, et al. A multicenter comparison of [18 F]flortaucipir, [18 F]RO948, and [18 F] MK6240 tau PET tracers to detect a common target ROI for differential diagnosis. *Eur J Nucl Med Mol Imaging* 2021; 48: 2295–2305.
17. Smith R, Strandberg O, Leuzy A, et al. Sex differences in off-target binding using tau positron emission tomography. *NeuroImage Clin* 2021; 31: 102708.
18. Mertens N, Michiels L, Vanderlinden G, et al. Impact of meningeal uptake and partial volume correction techniques on [18F]MK-6240 binding in aMCI patients and healthy controls. *J Cereb Blood Flow Metab* 2022; 42: 1236–1246.
19. Hanseuw BJ, Betensky RA, Jacobs HILL, et al. Association of amyloid and tau with cognition in preclinical Alzheimer disease: a longitudinal study. *JAMA Neurol* 2019; 76: 915–924.
20. Sanchez JS, Becker JA, Jacobs HIL, et al. The cortical origin and initial spread of medial temporal tauopathy in Alzheimer's disease assessed with positron emission tomography. *Sci Transl Med* 2021; 13: eabc0655.
21. Villain N, Chételat G, Grassiot B, et al. Regional dynamics of amyloid-β deposition in healthy elderly, mild cognitive impairment and Alzheimer's disease: a voxelwise PiB–PET longitudinal study. *Brain* 2012; 135: 2126–2139.
22. Blautzik J, Brendel M, Sauerbeck J, et al. Reference region selection and the association between the rate of amyloid accumulation over time and the baseline amyloid burden. *Eur J Nucl Med Mol Imaging* 2017; 44: 1364–1374.
23. Lowe VJ, Lundt ES, Senjem ML, et al. White matter reference region in PET studies of 11C-Pittsburgh compound B uptake: effects of age and amyloid-β deposition. *J Nucl Med* 2018; 59: 1583–1589.
24. Kameyama M, Ishibash K, Wagatsuma K, et al. A pitfall of white matter reference regions used in [18F] florbetapir PET: a consideration of kinetics. *Ann Nucl Med* 2019; 33: 848–854.
25. Schmidt ME, Chiao P, Klein G, et al. The influence of biological and technical factors on quantitative analysis of amyloid PET: Points to consider and recommendations for controlling variability in longitudinal data. *Alzheimers Dement* 2015; 11: 1050–1068.
26. Albert MS, DeKosky ST, Dickson D, et al. The diagnosis of mild cognitive impairment due to Alzheimer's disease: recommendations from the National Institute on Aging–Alzheimer's Association workgroups on diagnostic guidelines for Alzheimer's disease. *Alzheimers Dement* 2011; 7: 270–279.
27. Fischl B, Salat DH, Busa E, et al. Whole brain segmentation: automated labeling of neuroanatomical structures in the human brain. *Neuron* 2002; 33: 341–355.
28. Fischl B, van der Kouwe A, Destrieux C, et al. Automatically parcellating the human cerebral cortex. *Cereb Cortex* 2004; 14: 11–22.
29. Baker SL, Lockhart SN, Price JC, et al. Reference tissue-based kinetic evaluation of 18F-AV-1451 for tau imaging. *J Nucl Med* 2017; 58: 332–338.
30. Greve DN, Salat DH, Bowen SL, et al. Different partial volume correction methods lead to different conclusions: an (18)F-FDG-PET study of aging. *Neuroimage* 2016; 132: 334–343.
31. Veronese M, Rizzo G, Bertoldo A, et al. *Spectral analysis of dynamic PET Studies: a review of 20 years of method developments and applications*. London: Hindawi Limited.
32. Cunningham VJ and Jones T. Spectral analysis of dynamic PET studies. *J Cereb Blood Flow Metab* 1993; 13: 15–23.
33. Fan Z, Dani M, Femminella GD, et al. Parametric mapping using spectral analysis for 11C-PBR28 PET reveals neuroinflammation in mild cognitive impairment subjects. *Eur J Nucl Med Mol Imaging* 2018; 45: 1432–1441.

34. Veronese M, Tuosto M, Marques TR, et al. Parametric mapping for TSPO PET imaging with spectral analysis impulsive response function. *Mol Imaging Biol* 2021; 23: 560–571.
35. Veronese M, Rizzo G, Turkheimer FE, et al. SAKE: a new quantification tool for positron emission tomography studies. *Comput Methods Programs Biomed* 2013; 111: 199–213.
36. Logan J, Fowler JS, Volkow ND, et al. Graphical analysis of reversible radioligand binding from time – activity measurements applied to [N-11C-methyl]-(-)-cocaine PET studies in human subjects. *J Cereb Blood Flow Metab* 1990; 10: 740–747.
37. Logan J, Fowler JS, Volkow ND, et al. Distribution volume ratios without blood sampling from graphical analysis of PET data. *J Cereb Blood Flow Metab* 1996; 16: 834–840.
38. Ichise M, Liow J-S, Lu J-Q, et al. Linearized reference tissue parametric imaging methods: application to [11C] DASB positron emission tomography studies of the serotonin transporter in human brain. *J Cereb Blood Flow Metab* 2003; 23: 1096–1112.
39. Jack CR, Bennett DA, Blennow K, Contributors, et al. NIA. Toward a biological definition of Alzheimer’s disease. *Alzheimer’s & Dementia* 2018; 14: 535–562. AA Research Framework:
40. Jack CR, Wiste HJ, Botha H, et al. The bivariate distribution of amyloid- β and tau: Relationship with established neurocognitive clinical syndromes. *Brain* 2019; 142: 3230–3242.
41. Farrell ME, Jiang S, Schultz AP, et al. Defining the lowest threshold for Amyloid-PET to predict future cognitive decline and amyloid accumulation. *Neurology* 2021; 96: e619–e631.
42. Fleisher AS, Joshi AD, Sundell KL, et al. Use of white matter reference regions for detection of change in florbetapir positron emission tomography from completed phase 3 solanezumab trials. *Alzheimers Dement* 2017; 13: 1117–1124.
43. Rowe CC, Doré V, Krishnadas N, et al. Tau imaging with 18 F-MK6240 across the Alzheimer’s disease spectrum. DOI: 10.1101/2022.02.13.22270894.
44. Pascoal TA, Benedet AL, Tudorascu DL, et al. Longitudinal 18F-MK-6240 tau tangles accumulation follows Braak stages. *Brain* 2021; 144: 3517–3528.
45. Young CB, Landau SM, Harrison TM, et al. Influence of common reference regions on regional tau patterns in cross-sectional and longitudinal [18F]-AV-1451 PET data. *Neuroimage* 2021; 243: 118553.
46. Chen K, Roontiva A, Thiyyagura P, et al. Improved power for characterizing longitudinal amyloid- β PET changes and evaluating Amyloid-Modifying treatments with a cerebral white matter reference region. *J Nucl Med* 2015; 56: 560–566.